

Carbon Monoxide Hydrogenation over Gd(Fe/Mn)O₃ Perovskite-Type Catalysts

T. F. Sheshko^{a,*}, E. B. Markova^a, A. A. Sharaeva^a, T. A. Kryuchkova^a, I. A. Zvereva^b,
I. V. Chislova^b, and L. V. Yafarova^b

^aPeoples' Friendship University of Russia, Moscow, 117198 Russia

^bSt. Petersburg State University, St. Petersburg, 198504 Russia

*e-mail: sheshko-tf@rudn.ru

Received January 8, 2019; revised July 10, 2019; accepted August 9, 2019

Abstract—Catalytic properties of GdFeO₃ and GdMnO₃ perovskite-type oxides in CO hydrogenation processes is conducted. Complex oxides Gd(Fe/Mn)O₃ are synthesized by the sol–gel technology and characterized by X-ray diffraction, temperature-programmed reduction, and scanning electron microscopy. It is found that the iron-containing catalyst has fairly high catalytic characteristics; therefore, it provides lower temperatures of carbon monoxide hydrogenation. The presence of manganese in the catalyst leads to an increase in light olefin selectivity compared with the sample containing iron at the B-site. It is assumed that gadolinium cations are responsible for dissociative chemisorption, while iron and manganese cations are responsible for the formation of atomic hydrogen. The two catalysts exhibit resistance to carbon deposition.

Keywords: perovskites, hydrogenation, carbon monoxide, olefins, perovskite-type complex oxides, ferrites

DOI: 10.1134/S0965544119120107

Perovskite-type complex oxides with a general formula of ABO₃ (A is an alkaline, alkaline-earth, or rare-earth element; B is a transition metal) are used as catalysts for various organic synthesis processes. Owing to the structural stability of these oxides and the possibility of varying the cationic composition over a wide range, these materials can be adapted to a number of processes for the selective synthesis of reaction products. The high thermal stability and oxygen and ion conductivity make perovskites ideal candidates for use as catalysts for high-temperature reactions [1]. It was shown [2] that the substitution of metals at the A- and B-sites of the complex oxide structure can provide the reaction selectivity for the target product.

The activity of La_(1-y)Co_{0.4}Fe_{0.6}O_{3-δ} perovskites in carbon monoxide hydrogenation increased with a decrease in the lanthanum fraction in the systems [3]; the highest selectivity for C₂–C₄ olefins was exhibited by a La_(1-y)Co_{0.4}Fe_{0.6}O_{3-δ} catalyst, where y = 0.4, due to the formation of a Fe–Co metal alloy on the surface owing to the partial reduction of the complex oxide under the action of the reaction medium. The authors of [1] found that the substitution of strontium for lanthanum in perovskite catalysts of the La_{1-x}Sr_xCoO₃ type led to the inhibition of the Fischer–Tropsch synthesis process, which was attributed by the cited authors to a change in the complex oxide structure and the transition from a rhombohedral to less stable cubic

structure. A variation in the Co/Fe ratio and the La content in LaCo_xFe_(1-x)O₃ [4] also led to a change in the crystal structure type (rhombohedral, orthorhombic, cubic), which affected the formation of metal phases on the catalyst surface due to reduction and, as a consequence, influenced the C₂–C₄ olefin selectivity. The Co/La₂O₃-doped La₄Ga₂O₉ catalyst (LaCo_{1-x}Ga_xO₃ as a precursor) showed a high ethanol selectivity, stability, and resistance to sintering and carbon deposition in the Fischer–Tropsch synthesis using a simulated gas mixture comparable to bio-synthesis gas [5].

The effect of partial substitution of the metal at the A-sites of a perovskite-like Gd_{2-x}Sr_{1+x}Fe₂O₇ (x = 0, 0.1, 0.2, 0.3, 0.4) layered oxide was studied previously [6]. It was found that the nonisovalent substitution of Sr²⁺ for Gd³⁺ leads to distortion of the structure and implementation of the heterovalent state of iron atoms (Fe³⁺ and Fe⁴⁺), which affects the olefin selectivity in the CO hydrogenation process. It was shown that that Gd_{2-x}Sr_{1+x}Fe₂O₇ with x = 0.3 exhibited the highest selectivity for unsaturated hydrocarbons (ethylene and propylene) in carbon monoxide hydrogenation.

Light olefins, such as ethylene, propylene, and butylene, are commonly used for the synthesis of naphtha conversion products (e.g., solvents, paints, polymers). The conventional methods for the production of light olefins (pyrolysis and liquid-phase catalytic cracking of straight-run gasoline and the FCC

process) were not able to satisfy the high market demand because of the low olefin selectivity and the high cost of petroleum feedstocks [7]. In recent years, studies aimed at searching for alternative methods for the production of light olefins have been conducted [8–11]. The reforming of coal, natural gas, and biomass provides an alternative route for light olefin synthesis. Some processes, such as methanol to olefins (MTO) and syngas via dimethyl ether to olefins (SDTO) in the presence of zeolite catalysts have already been implemented in industry. The main disadvantages of these technologies are the high operating costs and the rapid catalyst deactivation [12].

The aim of this study is to compare the catalytic activity of GdFeO_3 and GdMnO_3 complex oxides containing different cations at the B-sites in carbon monoxide hydrogenation.

EXPERIMENTAL

Sample synthesis procedure. Initial reagents were reagent grade $\text{Gd}(\text{NO}_3)_3 \cdot 6\text{H}_2\text{O}$ (Specifications TU 6–09–4676–83), high-purity grade $\text{Mn}(\text{NO}_3)_2 \cdot 6\text{H}_2\text{O}$ and $\text{Fe}(\text{NO}_3)_3 \cdot 9\text{H}_2\text{O}$ (TU 6–09–02–553–96), citric acid, and an ammonia solution.

The $\text{Gd}(\text{Fe,Mn})\text{O}_3$ compounds were synthesized by the sol–gel method in accordance with the citrate–nitrate technique [13, 14]. $\text{Gd}(\text{NO}_3)_3 \cdot 5\text{H}_2\text{O}$ and $\text{Mn}(\text{NO}_3)_2 \cdot 6\text{H}_2\text{O}/\text{Fe}(\text{NO}_3)_3 \cdot 9\text{H}_2\text{O}$ compounds taken in a stoichiometric amount were dissolved in distilled water; the resulting solution was mixed with an aqueous solution of citric acid; after that, to maintain pH 6, an ammonia solution was added dropwise under permanent stirring. The prepared solution was held at a temperature of 353–363 K to obtain a wet gel, which was slowly heated in air to a temperature of 523 K, at which ignition and intense gas evolution were observed. After ignition, the sample was calcined with a gradual increase in temperature from 523 to 723 K for 30 min and then held at 723 K for 2 h. The resulting powders were crushed (homogenized) in an agate mortar, pelletized, and calcined in a muffle furnace at a temperature of 1073 K for 1 h.

Investigation procedures. The phase composition of the catalysts before and after catalytic tests was studied by X-ray powder diffraction analysis (Rigaku Mini-Flex II instrument) at room temperature ($\text{CuK}\alpha$ radiation, an angular range of $2\theta = 20^\circ\text{--}60^\circ$, a scan rate of $5^\circ\text{C}/\text{min}$). The crystalline phases were identified using the PDF2 database.

The morphology and chemical composition of the surface before and after catalytic processes were studied using an emission scanning microscope (Zeiss Merlin and Zeiss Supra 40VP) equipped with an energy dispersive spectroscopy system.

The specific surface area of the compounds before catalytic reactions was determined by nitrogen adsorp-

tion at -196°C (Quadratorb SI). Prior to adsorption measurements, all samples were degassed at 300°C for 5 h to remove residual moisture and other volatile substances.

The oxidation state of Fe and Mn was studied by X-ray photoelectron spectroscopy (Thermo Fisher Scientific Escalab 250Xi) using $\text{AlK}\alpha$ radiation ($\lambda = 0.1541\text{ nm}$) as an excitation source.

Catalytic testing procedure. Catalytic activity in carbon monoxide hydrogenation was tested in a U-shaped fixed-bed quartz flow reactor with a 100-mg weighed portion of the catalyst diluted with quartz (weight of 500 mg, a fraction of 0.25–0.5 nm) placed into it. The reactor was placed in a temperature-controlled furnace; temperature was measured/controlled using a K-type thermocouple placed into the center of the catalytic bed without direct contact. The process temperature was increased from 523 to 708 K. The reaction was run at a pressure of 1 atm and a gas mixture flow rate of 1.5 L/h ($\text{CO} : \text{H}_2 = 1 : 2$). In all tests, the samples were used without prereduction. Analysis of the reaction mixture above the catalyst surface was conducted on a Kristall 5000.2 gas chromatograph equipped with a stainless steel column filled with the Porapak Q sorbent and sequentially connected thermal conductivity and flame ionization detectors. The rate of formation of reaction products (specific catalytic activity) R ($\text{mol}/(\text{h g}_{\text{cat}})$) was determined from the constancy of chromatographic peaks.

Carbon monoxide conversion was calculated by the formula

$$X_i = \frac{n_{i,\text{inlet}} - n_{i,\text{outlet}}}{n_{i,\text{inlet}}} \times 100\%, \quad (1)$$

where $n_{i,\text{inlet}}$ and $n_{i,\text{outlet}}$ are the amount of carbon monoxide at the inlet and outlet of the reactor, respectively.

The rate of formation was calculated by the formula

$$R_i = \frac{K_x S_i w}{V_{\text{loop}} m_{\text{cat}}}, \quad (2)$$

where K_x is the correction coefficient for the i th reaction product; S_i is the peak area, mm^2 ; R_i is the rate of formation of the i th reaction product per gram of catalyst; w is the volume flow rate of the reaction mixture, 1–1.5 L/h; V_{loop} is the chromatograph loop volume, 0.001 L; and m_{cat} is the weight of the catalyst metal phase, g.

Reaction product selectivity was calculated by the formula

$$S_i = \frac{R_i}{\sum R_i} \times 100\%, \quad (3)$$

where R_i is the rate of formation of the i th reaction product per gram of catalyst, $\text{mol}/(\text{h g}_{\text{cat}})$ and $\sum R_i$ is the sum of the rates of formation of the i th reaction products per gram of catalyst, $\text{mol}/(\text{h g}_{\text{cat}})$.

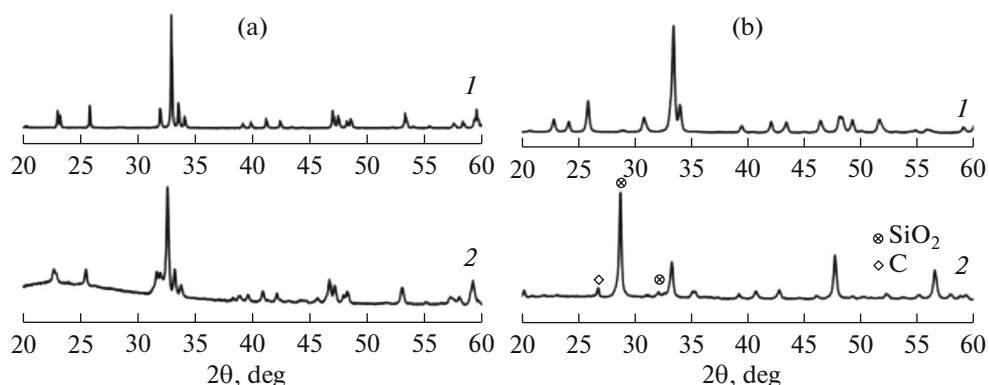


Fig. 1. XDR patterns of (a) GdFeO_3 and (b) GdMnO_3 oxides: (1) before and (2) after catalytic processes.

RESULTS AND DISCUSSION

The diffraction patterns of the samples measured before catalytic tests (Fig. 1) show that all the synthesized compounds obtained are single-phase materials, because the diffraction peaks are in good agreement with the data from the PDF2 database: GdFeO_3 (01-072-9908) and GdMnO_3 (01-070-9199). An analysis of the phase composition after catalytic tests shows that the phase composition of GdFeO_3 remains unchanged during reactions, while the diffraction pattern of GdMnO_3 shows the presence of C (PDF#00-041-1487); in addition, the presence of SiO_2 (PDF#01-077-1725), which was used to prevent the catalyst surface from sintering, is observed for the tested samples.

The specific surface area determined by the low-temperature nitrogen adsorption method (Brunauer–Emmett–Teller method) for GdFeO_3 and GdMnO_3 was 3.0 and 8.5 m^2/g , respectively.

Scanning electron microscopy data show that the synthesized compounds have similar morphologies and consist of crystalline particles with an average size of 100–200 nm (Fig. 2). However, a slight agglomeration of particles is observed after catalytic tests. The energy dispersive analysis of the surface of the studied compounds shows that, after catalytic processes, carbon is present on the sample surface; however, the quantitative content of carbon cannot be determined, because of its uneven distribution over the catalyst surface.

X-ray photoelectron spectroscopy studies of the catalysts showed that the GdFeO_3 compound comprises Fe in the 3⁺ state (Fe $2p_{3/2}$ binding energy of ~710.9 eV), while the GdMnO_3 compound comprises Mn in the 2⁺ and 3⁺ heterovalent state (Mn $2p_{3/2}$ binding energy of ~641.48 eV).

Carbon monoxide hydrogenation was run in a temperature range of 523–708 K at a CO : H_2 ratio of 1 : 2. Analysis of the content of the reactants in the gas phase at the catalyst surface showed that an intense

adsorption of CO occurs at room temperature, and the behavior of the curves is identical for the two samples (Fig. 3).

After establishment of the adsorption equilibrium, up to a temperature of 573 K, the composition of the gas phase (CO + H_2) remained almost unchanged, and the transition to the catalytic temperature range (596–708 K) was accompanied by the formation of CO_2 . This process was particularly pronounced in the presence of gadolinium ferrite; this fact can be apparently attributed to a more intense occurrence of the Bell–Boudoir reaction $2\text{CO} \rightarrow \text{CO}_2 + \text{C}$ to form the active carbon [15].

In addition, CO_2 can be formed during the reaction of an adsorbed CO_{ads} molecule either with the surface oxygen of perovskite (O_s) or with oxygen released during the dissociative adsorption of CO; that is, $\text{CO}_{\text{ads}} + \text{O}_\text{s} \rightarrow \text{CO}_2$ [15]. In the presence of sample 1 (GdMnO_3), the CO conversion was ~70% and varied only slightly with increasing temperature, while in the presence of sample 2 (GdFeO_3), the CO conversion was slightly lower—at a level of ~60% (Fig. 3c).

Since the behaviors of the curves describing the temperature dependences of CO conversion and CO content in the reaction mixture did not differ significantly for the studied catalysts, it can be assumed that only carbon particles formed during dissociative adsorption in the region of noncatalytic temperatures are involved in the formation of the reaction products.

In the presence of all the tested samples, the hydrogenation reaction products were C_1 – C_6 hydrocarbons; the main products were methane, ethylene, propylene, and butylene. The formation of all the products began even at 523 K and increased with increasing temperature; however, at $T > 623$ K, the rates of formation of C_3 – C_6 hydrocarbons decreased (Table 1).

A comparison of the rates of formation of the main products (methane, ethylene, butylene, CO_2) in the presence of the studied samples revealed that the replacement of Mn (sample 1) by Fe (sample 2) at the

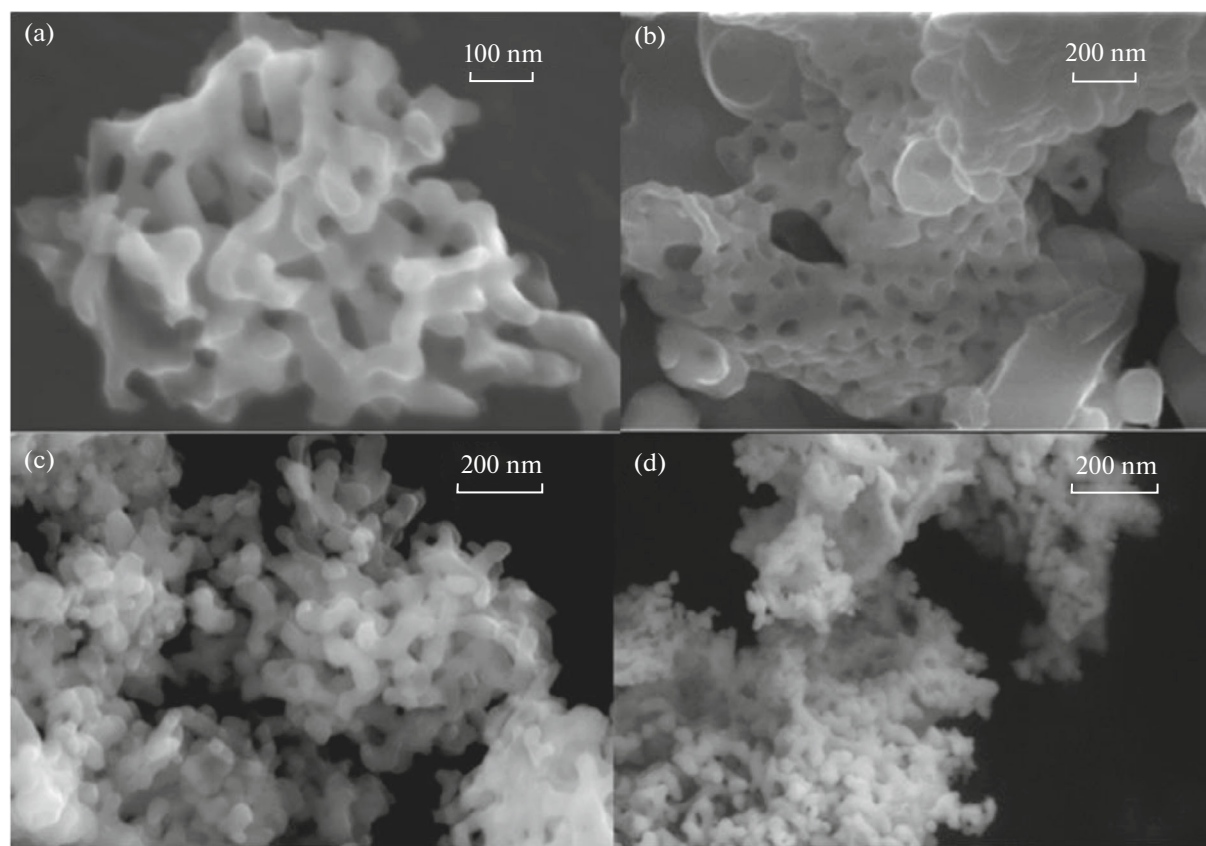


Fig. 2. SEM images of (a, b) GdFeO_3 and (c, d) GdMnO_3 : (a, c) before and (b, d) after catalytic reaction.

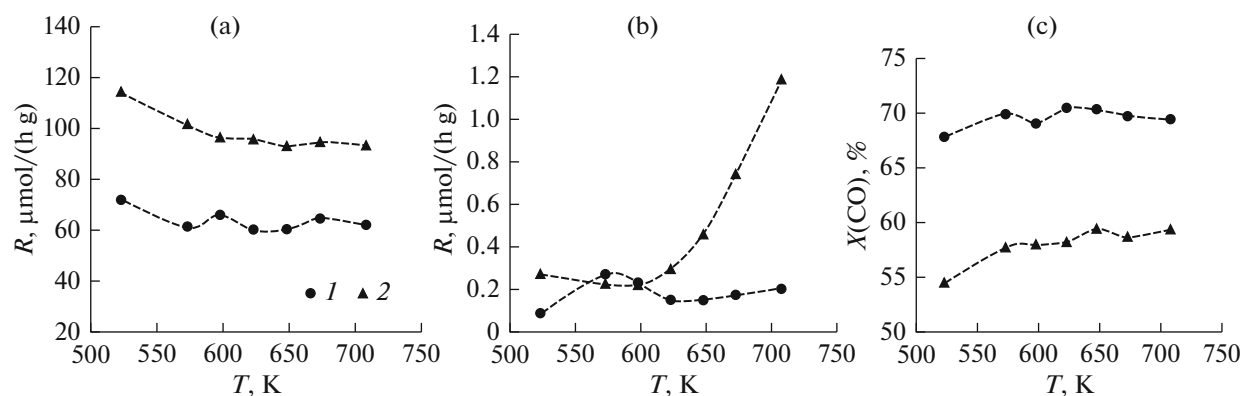


Fig. 3. Temperature dependences of (a) carbon monoxide and (b) carbon dioxide content in the gas phase during adsorption and hydrogenation and (c) temperature dependences of CO conversion at a $\text{CO} : \text{H}_2$ ratio of 1 : 2.

B-site of the perovskite structure causes a significant increase in specific catalytic activity, i.e., an increase in the rates of formation of the main reaction products (Table 1). Since catalytic synthesis occurs via the reaction of chemisorbed reagents, it is reasonable to expect correlation of the catalytic activity and selectivity of transition metals with both the absolute values of the heat of adsorption of CO and H_2 on the metal surface

and their difference [16]. The difference between the adsorption energies of CO and H_2 on the Fe surface is less than that on the Mn surface; these energies themselves are not extremely high; therefore, the energy barrier to the reaction of adsorbed CO and H_2 will be small. These values correlate well with the CO conversion obtained and specific catalytic activity of the samples.

Table 1. Rate of formation R of the main products of the hydrogenation reaction at a CO : H₂ ratio of 1 : 2

| Sample | T , K | $R(\text{CH}_4)$, $\mu\text{mol}/(\text{g h})$ | $R(\text{C}_2\text{H}_4)$, $\mu\text{mol}/(\text{g h})$ | $R(\text{C}_2\text{H}_6)$, $\mu\text{mol}/(\text{g h})$ | $R(\text{C}_3\text{H}_6)$, $\mu\text{mol}/(\text{g h})$ | $R(\text{C}_4\text{H}_8)$, $\mu\text{mol}/(\text{g h})$ | $R(\text{C}_4\text{H}_{10})$, $\mu\text{mol}/(\text{g h})$ | $R(\text{C}_5\text{H}_{10})$, $\mu\text{mol}/(\text{g h})$ |
|--------------------|---------|--|---|---|---|---|--|--|
| GdMnO ₃ | <600 | 1.08 | 0.27 | 0.07 | 0.05 | 2.39 | 0.03 | 1.21 |
| | >700 | 6.79 | 2.64 | 0.07 | 0.04 | 0.28 | 0.35 | 1.03 |
| GdFeO ₃ | <600 | 303.23 | 90.82 | 6.45 | 36.42 | 6.37 | 9.00 | 2.69 |
| | >700 | 2536.01 | 726.89 | 39.33 | 0 | 0.27 | 30.48 | 2.16 |

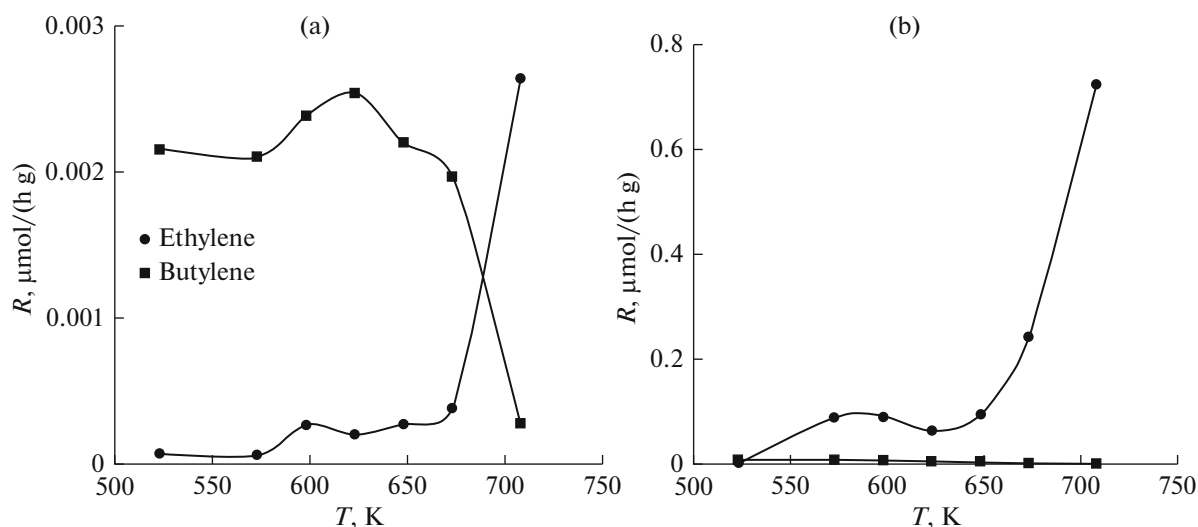
A variation in the catalyst composition led to a change in the quantitative ratio of hydrogenation products. For example, in the presence of the GdMnO₃ catalyst, the content of methane and light olefins in the reaction mixture at $T = 673$ K was 40 and 35%, respectively; in the case of complex oxides in which iron was completely replaced with manganese, the amount of methane increased to 71%, while the olefin content decreased to 26%; the fraction of C₅–C₆ hydrocarbons also decreased. It should be noted that, for manganese-containing sample 1, in the temperature range up to 673 K, the rates of formation of butylene were almost an order of magnitude higher than the rates of formation of ethylene (Fig. 4). Further increase in temperature provoked a decrease in the rates of formation of butylene and a significant increase in the rates of formation of ethylene. In the case of sample 2 (GdFeO₃), the amount of butylene was negligible (Fig. 4).

Earlier [17], it has been speculated that, during carbon oxide hydrogenation, iron-generated CH_x radicals can be transferred through the gas phase (the jump-over effect) to the manganese oxide surface, which hardly contains sorbed hydrogen; it is this place where the subsequent recombination of these radicals to olefins occurs. Difference in the catalytic activities of the

GdMnO₃ and GdFeO₃ samples can be associated with different diffusion rates of weakly bound atomic hydrogen across the catalyst surface (the spillover effect). Apparently, at low temperatures, in the presence of the manganese-containing samples, the CH_x radicals react with each other to form mostly butylene. An increase in the process temperature leads to an increase in the mobility of both the CH_x particles and atomic hydrogen; it is this factor that is responsible for an increase in the amount of the produced ethylene.

Calculations of total olefin selectivities during hydrogenation indicated that the introduction of manganese into the B-site of the perovskite lattice contributes to an increase in the process selectivity for light olefins (C₂–C₄), as evidenced by Fig. 5. Thus, at temperatures of 623–673 K, in the presence of the GdFeO₃ sample, the olefin selectivity was about 25%; in the case of the manganese-containing sample, selectivity achieved 80%, which is higher than the values described in [18, 19] for iron–manganese catalysts.

The processing of the test data in the linear coordinates of the Arrhenius equation made it possible to determine the effective activation energies for the formation of products and the logarithms of the pre-exponent characterizing the number of active sites.

**Fig. 4.** Temperature dependences of the rates of ethylene and butylene formation over (a) GdMnO₃ and (b) GdFeO₃.

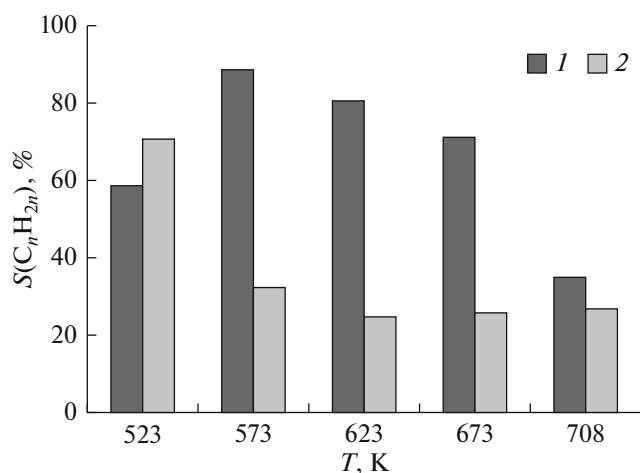


Fig. 5. Light olefins selectivity over (1) GdMnO_3 and (2) GdFeO_3 during hydrogenation at a $\text{CO} : \text{H}_2$ ratio of 1 : 2.

The effective activation energies for the formation of methane $E_a^{\text{eff}}(\text{CH}_4)$ were 67 and 70 kJ/mol for samples 1 and 2, respectively (negligible differences between 1 and 2), while $\ln K_0(\text{CH}_4)$ for sample 1 was significantly lower than that for sample 2 (−1.05 and 5.7, respectively). Apparently, a decrease in the number of active sites affected the decrease in the rates of formation of products in the presence of the manganese-containing sample. An opposite tendency was observed for the formation of olefins: at close $\ln K_0$ values (3.46 and 3.49), the effective activation energies for sample 1 were higher (98 kJ/mol vs. 65 kJ/mol for sample 2).

Thus, the comprehensive physicochemical study of the samples after catalytic processes has shown the following:

(i) Temperature and reaction medium do not affect the structure of the GdBO_3 ($\text{B} = \text{Fe}, \text{Mn}$) complex oxide; the phase composition of the catalyst remains unchanged.

(ii) The high-temperature process leads to particle agglomeration, which results in a decrease in the specific surface area of the samples. Elemental analysis has shown the presence of carbon on the surface of the studied perovskites; in addition, deposition occurs unevenly. However, since all the catalytic characteristics of the complex oxides are maintained for a long time (50 h), it can be assumed that most of the surface carbon is involved in the reaction and exhibits activity.

(iii) The substitution of manganese for iron in the GdFeO_3 catalyst leads, on the one hand, to a change in CO conversion and, on the other hand, to a significant increase in olefin selectivity in the cohydrogenation of carbon oxides. It has been speculated that iron-generated CH_x radicals are transferred through the gas phase (the jumpover effect) to the manganese oxide

surface, which hardly contains sorbed hydrogen; it is this place where the subsequent recombination of these radicals to olefins occurs. Differences in the catalytic activity of the samples are attributed to different diffusion rates of weakly bound atomic hydrogen (H_1) across the catalyst surface (the spillover effect). Our results are in good agreement with this assumption: at low temperatures, in the presence of the manganese-containing samples, the CH_x radicals react with each other to form mostly butylene. An increase in the process temperature leads to an increase in the mobility of both CH_x particles and atomic hydrogen; it is this factor that is responsible for an increase in the amount of the produced ethylene. The nature of the 3d metal in GdBO_3 does not affect the coking rate of the catalysts; the two catalyst systems showed resistance to carbon deposition.

ACKNOWLEDGMENTS

The physicochemical studies were conducted using the equipment of the Thermogravimetric and Calorimetric Research Center, the Center for X-ray Diffraction Studies, the Center for Physical Methods of Surface Investigation, and the Interdisciplinary Resource Center for Nanotechnology of the St. Petersburg State University Research Park.

FUNDING

This work was supported by Russian Foundation for Basic Research, project no. 17-03-00647.

Preparation of the publication was supported by the RUDN University Program 5-100.

CONFLICT OF INTEREST

The authors declare that there is no conflict of interest regarding the publication of this manuscript.

ADDITIONAL INFORMATION

T.F. Sheshko, ORCID: <https://orcid.org/0000-0003-4176-4085>

E.B. Markova, ORCID: <https://orcid.org/0000-0003-2735-2893>

A.A. Sharaeva, ORCID: <https://orcid.org/0000-0001-6465-7368>

T.A. Kryuchkova, ORCID: <https://orcid.org/0000-0001-6810-9756>

I.A. Zvereva, ORCID: <http://orcid.org/0000-0002-6898-3897>

I.V. Chislova, ORCID: <http://orcid.org/0000-0001-5212-5014>

L.V. Yafarova, ORCID: <http://orcid.org/0000-0001-7572-2209>

REFERENCES

1. M. Ao, G. H. Pham, V. Sage, and V. Pareek, *J. Mol. Catal. A: Chem.* **416**, 96 (2016).
2. N. T. Thao and L. T. Son, *J. Sci.: Adv. Mater. Devices* **1**, 337 (2016).
3. L. Bedel, A. Roger, J. Rehspringer, Y. Zimmermann, and A. Kiennemann, *J. Catal.* **235**, 279 (2005).
4. L. Bedel, A. C. Roger, J. L. Rehspringer, and A. Kiennemann, *Stud. Surf. Sci. Catal.* **147**, 319 (2004).
5. N. Escalona, S. Fuentealba, and G. Pecchi, *Appl. Catal., A* **381**, 253 (2010).
6. T. F. Sheshko, T. A. Kryuchkova, Yu. M. Serov, I. V. Chislova, and I. A. Zvereva, *Cat. Ind.* **9** (2), 162 (2017).
7. A. Bakhtyari, M. A. Makarem, and M. R. Rahimpour, in *Bioenergy Systems for the Future: Prospects for Biofuels and Biohydrogen*, Ed. by F. Dalena, A. Basile, and C. Rossi (Woodhead Publishing, Sawston, 2017), pp. 87–148.
8. S. Golestan, A. A. Mirzaei, and H. Atashi, *Int. J. Hydrogen Energy* **42**, 9816 (2017).
9. M. Arsalanfar, A. A. Mirzaei, H. R. Bozorgzadeh, A. Samimi, and R. Ghobadi, *J. Ind. Eng. Chem* **20**, 1313 (2014).
10. J. Zhang, X. Wang, L. Ma, X. Yu, Q. Ma, S. Fan, and T. Zhao, *J. Fuel Chem. Tech.* **45** (12), 1489 (2017).
11. J. Zhang, L. Ma, S. Fan, T.-S. Zhao, and Y. Sun, *Fuel* **109**, 116 (2013).
12. M. Zhao, Y. Cui, J. Sun, and Q. Zhang, *Catal. Today* **316**, 142 (2018).
13. I. V. Chislova, A. A. Matveeva, A. V. Volkova, and I. A. Zvereva, *Glass Phys. Chem.* **37** (6), 653 (2011).
14. L. V. Yafarova, I. V. Chislova, I. A. Zvereva, T. A. Kryuchkova, V. V. Kost, and T. F. Sheshko, *J. Sol–Gel Sci. Technol.* (2019).
<https://doi.org/10.1007/s10971-019-05013-3>
15. A. L. Lapidus and A. Yu. Krylova, *Russ. Khim. Zh.* **44** (1), 43 (2000).
16. P. C. Keith, *Oil Gas J.* **45**, 102 (1946).
17. T. F. Sheshko and Yu. M. Serov, *Russ. J. Phys. Chem. A* **86** (2), 283 (2012).
18. J. Wenter, M. Kaminsky, G. L. Geoffroy, and M. A. Vannice, *J. Catal.* **105**, 155 (1987).
19. J. J. Venter and M. A. Vannice, *Catal. Lett.* **7**, 219 (1990).

Translated by M. Timoshinina